

# Identification and validation of a driver steering control model incorporating human sensory dynamics

C. J. Nash and D. J. Cole

Department of Engineering, University of Cambridge, Cambridge, UK

## ARTICLE HISTORY

Compiled February 20, 2019

## ABSTRACT

Most existing models of driver steering control do not consider the driver's sensory dynamics, despite many aspects of human sensory perception having been researched extensively. The authors recently reported development of a driver model that incorporates sensory transfer functions, noise and delays. The present paper reports the experimental identification and validation of this model. An experiment was carried out with five test subjects in a driving simulator, aiming to replicate a real-world driving scenario with no motion scaling. The results of this experiment are used to identify parameter values for the driver model, and the model is found to describe the results of the experiment well. Predicted steering angles match the linear component of measured results with an average 'variance accounted for' of 98% using separate parameter sets for each trial, and 93% with a single fixed parameter set. The identified parameter values are compared with results from the literature and are found to be physically plausible, supporting the hypothesis that driver steering control can be predicted using models of human perception and control mechanisms.

## KEYWORDS

driver, vehicle, steering, control, perception, model, identification, vestibular, simulator, simulation

## 1. Introduction

The computational tools available to automotive engineers allow vehicle dynamics to be predicted accurately, so that quantitative metrics for vehicle design can be defined. However, driver perception and control mechanisms are still poorly understood, therefore it is difficult to predict the effects of design changes on the closed-loop driver-vehicle system. There is significant motivation for developing driver models which allow quantitative analysis and optimisation of the driver-vehicle system without relying on track testing and subjective driver feedback. Various models of driver steering control exist [1,2], however few consider the driver's sensory dynamics. The role of sensory dynamics during driving can be placed within the 'two-level' model proposed by Donges [3]. In this model a feedforward controller observes the road ahead, plans a trajectory for the vehicle and calculates the required steering inputs, while a feedback controller corrects for disturbances about this planned trajectory. The feedforward controller operates based on inputs from the visual system alone, as modelled by optimal 'preview' controllers [4,5]. The feedback task involves using estimates of the vehicle

states to correct for disturbances around the planned path. Drivers cannot know all the vehicle states with complete accuracy, but instead take noisy, filtered, delayed measurements of different sensory variables and use these to estimate the information required to control the vehicle. The main sensory systems used for the feedback task are the visual, vestibular and somatosensory systems.

Bigler [6] used results from the literature on human sensory perception to develop a driver steering control model incorporating sensory dynamics, noise and delays. Parameter values for the sensory channels were determined mainly from published experiments performed on each channel in isolation. However, recent studies have shown that sensory thresholds increase significantly during an active control task [7,8] and in the presence of additional sensory stimuli [9–11]. An active control task such as driving requires attention to be shared between the task itself and the perception of concurrent sensory stimuli, in contrast with passive perception tasks where the subject is concentrating solely on one sensory stimulus. Nash and Cole [12], building upon the work of Bigler [6], and upon a review of the literature [13], developed an improved driver model incorporating sensory dynamics. Preliminary analysis of this model was carried out [14] using published results from an experiment in a flight simulator [15] to validate the modelling approach for an aeroplane control task.

The aim of the work described in the present paper is to identify and validate the driver model presented in [12]. Experimental data is collected from a driving simulator experiment measuring steering control behaviour. An important feature of the work is that parameter values of the driver’s sensory channels are identified from data measured during an active driving task, rather than from separate passive perception tasks. The driver model is described in full in [12], and is summarised in Section 2. The design of the driving simulator experiment is described in Section 3 and the identification procedure is outlined in Section 4. The results are presented in Section 5 and discussed in Section 6. The conclusions are given in Section 7.

## 2. Driver steering control model

The parametric driver steering control model incorporating human sensory dynamics and reported in [12] is summarised in this section to the extent that it is necessary to understand the rest of the present paper. The model is built around an optimal control strategy, hypothesising that drivers achieve close to the best possible performance within the limitations of their sensory and motor systems. Driving a vehicle is a complicated task involving many physical and neural processes, so various simplifying assumptions are made. These assumptions could be removed when more is known about the role of sensory dynamics in the core driving task. The scope of the model does not extend to speed choice or control, therefore only vehicles travelling at constant longitudinal speed are considered. However, the principles behind this model could be extended to include variable-speed vehicles. The task of trajectory planning and optimisation is also not modelled; the driver is assumed to follow a given target path of negligible width. This limitation could be overcome by cascading a trajectory planning model which calculates a desired trajectory based on the road geometry [16] with the steering control model which attempts to follow this trajectory in the presence of disturbances. To reduce the computational effort involved in simulating the model and provide efficient mathematical solutions, linear dynamics are used to model the driver-vehicle system. Tyre friction characteristics are not considered, and the yaw angle of the vehicle is assumed to be small.

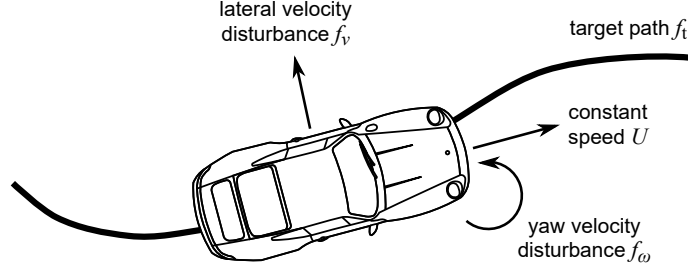


**Figure 1.** Summary of steering task described by the driver model. The driver follows a target path  $f_t$  while compensating for disturbances  $f_v$  and  $f_\omega$ .

The steering task described by the model is shown in Figure 1, combining the feedforward and feedback tasks described by the two-level model [3]. The feedforward task involves following the target path  $f_t$ , and the feedback task involves compensating for random disturbances  $f_v$  and  $f_\omega$ . These disturbances may come from a variety of sources such as wind gusts, vehicle nonlinearities and driver noise, however they can be modelled as additive disturbances referred to the vehicle lateral velocity  $v$  and yaw velocity  $\omega$ . The target and disturbance signals  $f_t$ ,  $f_v$  and  $f_\omega$  are collectively known as forcing functions, as under controlled conditions they can be synthesised artificially to identify different loops of the driver-vehicle control system [15]. It is assumed that the aim of the driver is to minimise the tracking error between the vehicle lateral displacement and the target path.

The structure of the parametric model is shown in Figure 2. The plant describes the system controlled by the driver, including the vehicle dynamics and the driver's neuromuscular dynamics and sensory systems. The driver's control strategy follows the linear quadratic Gaussian (LQG) framework, combining a linear quadratic regulator (LQR) with a Kalman filter to give statistically optimal control actions and state estimates based on the driver's internal model of the plant. Previous studies have used an LQR controller to model driver steering control while following a target path [4,5], hypothesising that an experienced driver will learn to steer in an approximately optimal fashion. Various studies have found evidence that humans combine visual and vestibular information optimally [17–19], and humans have been found to use internal models to assist with motor control tasks [20]. A Kalman filter uses an internal model to achieve optimal state estimation in the presence of additive white noise. Sections 2.1 to 2.4 describe the various components of the driver model; a full mathematical derivation is presented in [12].

## 2.1. Plant

The plant describing the dynamics of the system controlled by the driver is shown in Figure 3. The driver's internal model is assumed to be a perfect representation of the true plant. The plant input  $\hat{\delta}$  plus process noise  $w$  is filtered by the driver's neuromuscular dynamics, giving the steering angle  $\delta$ . Forcing functions  $f_t$ ,  $f_v$  and  $f_\omega$  are generated by filtering white noise plant inputs  $w_t$ ,  $w_v$  and  $w_\omega$ , and added to the vehicle's lateral velocity  $v$  and angular velocity  $\omega$ . The driver previews the upcoming target  $f_t$ , with measurements delayed by a visual delay  $\tau_{vi}$  to give perceived displacements  $e_{vi}$ . The vehicle lateral acceleration and angular velocity are sensed through the otoliths and semi-circular canals (SCCs), with a vestibular delay of  $\tau_{ve}$  in both cases, giving perceived lateral acceleration  $a_{ve}$  and angular velocity  $\omega_{ve}$ . The plant

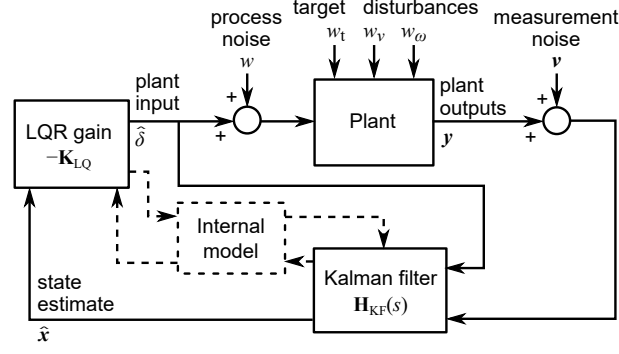


**Figure 2.** Structure of driver steering control model. Target and disturbance signals are input as white noise  $w_t$ ,  $w_v$  and  $w_\omega$ , then filtered in the plant. The plant input  $\hat{\delta}$  and outputs  $y$  are perturbed with process and measurement noise  $w$  and  $v$ , so a Kalman filter estimates the plant states  $\hat{x}$ . An LQR controller computes an optimal plant input  $\hat{\delta}$ .

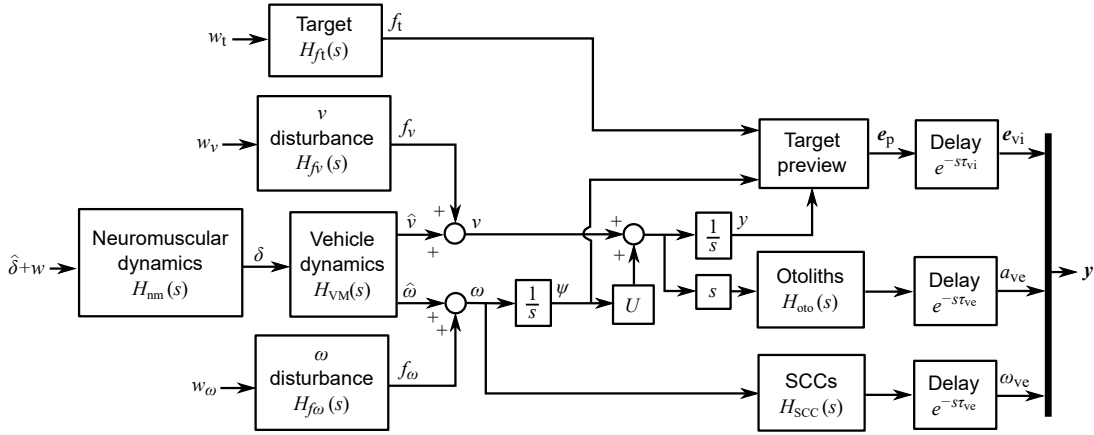


**Figure 3.** Structure of plant in the driver model. The plant describes the dynamics controlled by the driver, including the vehicle dynamics, driver’s neuromuscular and sensory dynamics, and target and disturbance filters.

is modelled in discrete time with sample time  $T_s$ , allowing delays to be implemented explicitly using a shift register.

A ‘preview’ model is used to describe the driver’s visual perception of the upcoming target path [4,5]. The driver previews future values of the target path up to the preview horizon  $T_p$  as shown in Figure 4. The previewed displacements  $e_{pn}(k)$  for  $n = 0, 1, \dots, N_p$ , where  $N_p = T_p/T_s$ , are:

$$e_{pn}(k) = f_t(k+n) - y(k) - nUT_s\psi(k) \quad (1)$$

assuming small yaw angles  $\psi$ . The vehicle is defined in [12] as a two degree-of-freedom single-track model moving at constant speed, discretised using a zero-order-hold method.

## 2.2. LQR controller

For a time-invariant linear plant an LQR controller can be calculated, consisting of a gain vector  $\mathbf{K}_{LQ}$  which acts on the plant states to give an optimal plant input  $\hat{\delta}$ ,

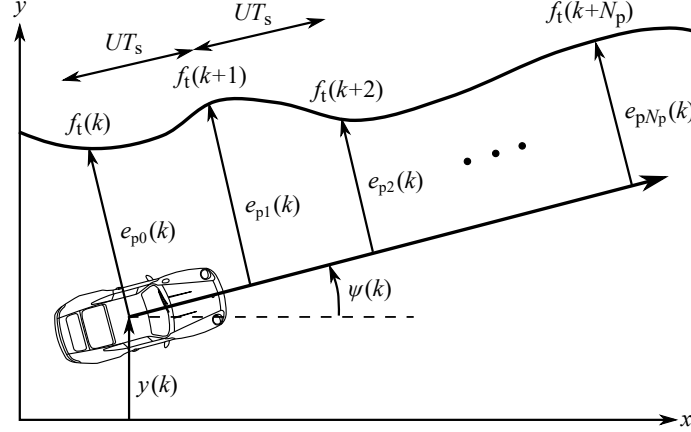


**Figure 4.** Model of the driver's visual preview of the target path. The driver measures lateral displacements of the target path relative to a line projected forward from the vehicle. Measurements are taken at intervals of  $UT_s$  up to a prediction horizon  $N_p = T_p/T_s$  time steps ahead.

which minimises a cost function  $J$ . Additive white noise does not affect the optimal solution, so the white noise plant inputs  $w$ ,  $w_t$ ,  $w_v$  and  $w_\omega$  can be ignored. The cost function incorporates costs on the tracking error  $e_{p0}$  and the plant input  $\hat{\delta}$ , weighted by  $q_e$  and  $q_\delta$ :

$$J = \sum_{k=0}^{\infty} \left\{ q_e e_{p0}(k)^2 + q_\delta \hat{\delta}(k)^2 \right\} \quad (2)$$

Previous studies have included costs on yaw angle error [4,5], and it is also possible to add additional terms such as steering velocity to the cost function. However for simplicity only two costs are included. The optimal solution only depends on the relative weightings, therefore  $q_e$  is set to  $1 \text{ m}^{-2}$ . As the steering cost is placed on  $\hat{\delta}$  rather than  $\delta$ , the cost on steering inputs is shaped by the neuromuscular transfer function  $H_{nm}(s)$ . The optimal gain  $\mathbf{K}_{LQ}$  can be found using the Matlab function *dlqr*.

### 2.3. Kalman filter

The LQR gain  $\mathbf{K}_{LQ}$  multiplies the plant states  $\mathbf{x}(k)$  to give an optimal plant input  $\hat{\delta}$ . However, the driver only has access to measurements of the plant outputs  $\mathbf{y}$ , perturbed by process and measurement noise  $w$  and  $\mathbf{v}$ . Therefore, a Kalman filter is used to compute an optimal estimate of the plant states based on the computed plant input and noisy measurements of the plant outputs. The noise covariance matrices are given by:

$$\mathbf{Q}_{KF} = \text{diag} \left( [W^2 \quad W_v^2 \quad W_\omega^2 \quad W_t^2] \right) \quad (3)$$

$$\mathbf{R}_{KF} = \text{diag} \left( [V_p^2 \times \mathbf{1}_{(1, N_p+1)} \quad V_a^2 \quad V_\omega^2] \right) \quad (4)$$

where  $W^2$ ,  $W_v^2$ ,  $W_\omega^2$  and  $W_t^2$  are the variances of the process noise  $w$  and the disturbance and target white noise inputs  $w_v$ ,  $w_\omega$  and  $w_t$ ;  $V_p^2$ ,  $V_a^2$ , and  $V_\omega^2$  are the variances of the measurement noise added to the plant outputs  $e_{vi}$ ,  $a_{ve}$ , and  $\omega_{ve}$ ; and  $\mathbf{1}_{(1, N_p+1)}$  is a column vector of  $(N_p + 1)$  ones.

This model assumes that the measurement noise has the same variance for all previewed target path displacements  $e_{vi}$ . Previous studies have accounted for an increase in noise with distance from the observer and eccentricity from the gaze direction [6], however there is a lack of research into how drivers view the geometry of an upcoming target path. The assumption of constant measurement noise  $V_p$  across all previewed displacements, while clearly a simplification, is not found to affect the fit to experimental results significantly. A time-invariant Kalman filter  $\mathbf{H}_{KF}(s)$  can be calculated for this system using the Matlab function *kalman*. The state estimate  $\hat{\mathbf{x}}$  can then be found from:

$$\hat{\mathbf{x}}(s) = \mathbf{H}_{KF}(s) \{ \hat{\delta}(s) \quad \mathbf{y}(s) \}^T \quad (5)$$

#### 2.4. Model transfer functions and parameters

As explained in Section 1, previous studies reviewed in [13] have shown that measurements of sensory perception taken in passive conditions may not be applicable to active control tasks such as driving [7–11]. Therefore, most of the parameters of the model are found using an identification procedure to fit to experimental results. However, the forms of some of the transfer functions can be fixed using results from the literature. Models of the vestibular system are taken from [21]:

$$H_{SCC}(s) = \frac{458.4s^2}{(80s + 1)(5.73s + 1)} \quad (6)$$

$$H_{oto}(s) = \frac{0.4(10s + 1)}{(5s + 1)(0.016s + 1)} \quad (7)$$

Drivers' neuromuscular dynamics are approximated by a second-order filter:

$$H_{nm}(s) = \frac{\omega_{nm}^2}{s^2 + 2\zeta_{nm}\omega_{nm}s + \omega_{nm}^2} \quad (8)$$

Pick and Cole [22] studied drivers' neuromuscular dynamics by applying torque disturbances to a steering wheel and found values of  $\omega_{nm} = 5.65$  rad/s and  $\zeta_{nm} = 0.43$  for drivers with relaxed arms and  $\omega_{nm} = 23.2$  rad/s and  $\zeta_{nm} = 0.24$  with tensed arms. It is unclear which is more appropriate for driver steering models, as drivers' arms may be partially tensed, therefore  $\omega_{nm}$  and  $\zeta_{nm}$  are identified to fit experimental data.

The values of some of the remaining parameters, such as the vehicle dynamics and the spectra and amplitudes of the forcing functions, are given by the experimental conditions. However various other parameters values must be identified, including the steering cost weight  $q_\delta$ , preview time  $T_p$ , the visual and vestibular delays  $\tau_{vi}$  and  $\tau_{ve}$ , noise amplitudes  $W$ ,  $V_a$ ,  $V_\omega$  and  $V_p$ , and neuromuscular parameters  $\omega_{nm}$  and  $\zeta_{nm}$ . If the driver previews the upcoming target path they should be able to compensate for their internal latencies to follow the target without any delay. However, preliminary analysis of the experimental results showed that drivers sometimes steered earlier than expected, as if they were following a 'shifted' version of the target  $f_t$ . This could be because the drivers aligned a different part of the car with the target other than the centre of mass. An additional time constant  $T_t$  is therefore included to model this effect, such that the driver attempts to follow  $f_t(t - T_t)$  rather than  $f_t(t)$ . In total there are eleven parameters which are neither determined by the experimental conditions

nor fixed using results from the literature, and these are found using the identification procedure described in Section 4.

### 3. Steering control experiment

A model of driver steering behaviour based on the dynamics of human sensory systems is presented in Section 2. To investigate how sensory information is used during driving, an experiment was carried out to provide data which can be used to identify values for the parameters of this model. A similar parameter identification procedure has previously been used in [14] to fit the model to an experiment carried out by pilots in a flight simulator [15]. The new experiment was designed following similar principles to measure driver steering control in a combined target-following and disturbance-rejection task. The experiment was carried out in a driving simulator, rather than a real vehicle on a test track, due to the control that this allows over the experimental set-up. Driving simulators have limited available travel, so the vehicle motion is usually scaled down or filtered to fit within these physical limitations. This results in a conflict between the information perceived by the visual and vestibular systems. There is some disagreement in the literature as to how sensory conflicts are perceived by humans [13]. Therefore, to ensure that the drivers used their sensory systems in the simulator in the same way as they would in a real vehicle, the vehicle motion was designed to fit within the simulator limits without any scaling or filtering. (A separate set of experiments was performed to investigate and model the effect of sensory conflicts on driver steering behaviour, these are reported in [23].)

#### 3.1. Steering control task

The steering control task carried out in the experiment was the same as the task described by the model in Section 2 (shown in Figure 1). The vehicle moved at constant longitudinal speed  $U$  and the drivers were asked to follow a target lateral displacement  $f_t$  as closely as possible. Disturbances  $f_v$  and  $f_\omega$  were added to the lateral velocity and yaw angular velocity of the vehicle as shown in Figure 3. The target and disturbance forcing function signals  $f_t$ ,  $f_v$  and  $f_\omega$  were generated by filtering Gaussian white noise to match the assumptions made in the driver model. White noise signals  $w_t$ ,  $w_v$  and  $w_\omega$  were generated in discrete time by choosing random numbers from a zero-mean normal distribution. The variances  $W_t^2$ ,  $W_v^2$  and  $W_\omega^2$  of these signals were adjusted between trials, as discussed in Section 3.3.

The forcing functions were tuned during preliminary testing to ensure that the amplitudes were as large as possible without exceeding the simulator limits, and to ensure that a large range of frequencies was included without becoming uncomfortable for the driver. The spectrum of the target forcing function  $f_t$  was defined by combining a high-pass filter, to attenuate low frequencies and ensure that the target path was within the simulator limits, with a low-pass filter to restrict the bandwidth of the target:

$$H_{f_t}(s) = \left( \frac{s}{s + 0.1} \right)^2 \left( \frac{2}{s + 2} \right)^2 \quad (9)$$

The spectra of  $f_v$  and  $f_\omega$  were chosen so that, in the absence of any steering, the vehicle's lateral displacement  $y$  would have the same spectrum as  $f_t$ . This was achieved

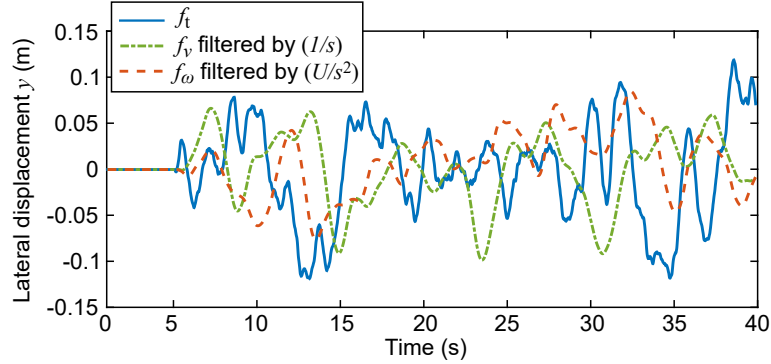


**Figure 5.** First 40 s of the forcing functions used in Trial A7. Disturbance forcing functions are filtered to show their effect on the vehicle lateral displacement.

by multiplying  $H_{f_t}(s)$  by  $s$  and  $H_{f_t}(s)$  by  $s^2/U$ , however this resulted in large-amplitude high-frequency components which caused very large velocities and accelerations. Therefore, the spectra were multiplied by an additional low-pass filter with cutoff frequency 3 rad/s:

$$H_{f_v}(s) = \left( \frac{3}{s+3} \right)^2 s H_{f_t}(s) \quad (10)$$

$$H_{f_\omega}(s) = \left( \frac{3}{s+3} \right)^2 \left( \frac{s^2}{U} \right) H_{f_t}(s) \quad (11)$$

Examples of the forcing functions used in one of the trials are shown in Figure 5.

### 3.2. Simulation conditions

A moving-base driving simulator was used for the experiment, with a high-fidelity visual display and a high-bandwidth motion platform which applied physical feedback to the driver. The lateral and yaw motion applied to the driver by the platform was not scaled or filtered in any way during the experiment. Therefore the lateral and yaw motion that was sensed visually, and the lateral and yaw motion that was sensed by the vestibular organs, were identical. In contrast, no longitudinal motion was applied to the driver by the platform, although longitudinal motion was presented on the visual display. However, because the human sensory system cannot detect constant longitudinal motion except visually, the driver would not have been aware of the absence of longitudinal motion of the platform, and their driving strategy would not have been affected. Simulated engine noise was played to mask the sounds of the motion platform. Suitable vehicle parameter values were found by fitting the steering response of the single-track model to the high-accuracy nonlinear vehicle model employed on the simulator. The aim was to find a linear model with a realistic overall steering response, rather than choosing each parameter separately based on measurements of a vehicle's physical properties. For the experiment, two vehicle speeds were chosen, a 'fast' vehicle with  $U = 40$  m/s and a 'slow' vehicle with  $U = 10$  m/s, which gives larger amplitudes of yaw motion without exceeding the lateral displacement limits of the simulator. The parameter values for the two vehicles are given in Table 1.

Previous experiments carried out by pilots used a visual display consisting of a

**Table 1.** Vehicle parameter values used in experiment, for the single-track model defined in [12].  $G$  is the steering gear ratio.

	$m$	$l_f$	$l_r$	$C_f$	$C_r$	$I$	$G$	$U$
<b>Units</b>	kg	m	m	kN/rad	kN/rad	kgm <sup>2</sup>	–	m/s
<b>Slow (S)</b>	650	1.85	1.65	100	230	450	30	10
<b>Fast (F)</b>	650	1.85	1.65	100	230	450	150	40

screen which showed a line representing the target aeroplane pitch angle and a cross-hair showing the actual pitch angle [15]. This display did not give the pilots any information about future values of the target angle. In contrast, drivers are usually able to see the road ahead of them, previewing the upcoming target path as shown in Figure 4. This allows them to compensate for delays in the visual feedback loop by planning steering actions in advance. Two types of visual display were designed for the experiment, one which allowed the driver to preview the upcoming target path in order to replicate a more realistic driving scenario, and one without preview to allow delays in the visual system to be investigated. Examples of the two displays are shown in Figure 6. In both cases the vehicle moved along a straight road, with objects such as trees and buildings next to the road for use as visual cues to speed and depth. In the ‘no preview’ case, a straight target line moved laterally across the road, with the lateral displacement of each point on this line equal to  $f_t(t)$  at time  $t$ . This allowed the driver to see the current value of  $f_t$  without any information about future values of the target. In the preview case the target line was fixed to the road, allowing the driver to see the upcoming target.

In a real vehicle, lateral forces generated by the tyres on the front axle are communicated to the driver through torque at the steering wheel, and this can give the driver useful information about the vehicle states. The driver model does not currently take account of steering torque feedback, therefore the steering system was modelled as parallel spring and damper, with transfer function:

$$H_{\text{STF}}(s) = k_{\text{STF}} + c_{\text{STF}}s \quad (12)$$

between steering angle and resistive torque. This provided some resistance to steering, however it didn’t give the driver any information about the vehicle states. The stiffness  $k_{\text{STF}}$  was set to 8 Nm/rad and the damping coefficient  $c_{\text{STF}}$  to 1 Nms/rad. The reason for omitting feedback of lateral tyre forces at this stage of the model development is to limit the number of model parameters required to be identified; experimental identification generally becomes more difficult as the number of unknown parameter values increases. Drivers’ perception of more sophisticated torque feedback will be investigated in the future and incorporated into the driver model.

### 3.3. Experiment procedure and trials

The experiment consisted of fourteen trials, each of 120 s duration, with a range of conditions designed to explore different aspects of the driver’s control strategy. The conditions are summarised in Table 2. Various forcing function combinations were tested with the slow and fast vehicles, with or without preview. For trials with no

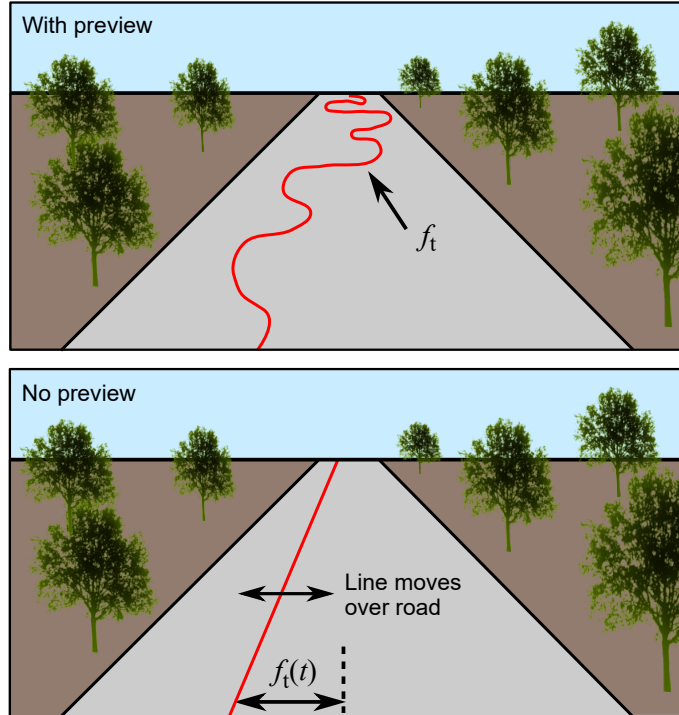


**Figure 6.** Visual display examples, with and without preview. Note that the simulator display was much higher fidelity than these examples.

target (marked **0** in the preview column) the ‘preview’ and ‘no preview’ models are equivalent. There were five test subjects in total, all male and aged between 24 and 30. All five drivers possessed driving licences and had at least six years experience driving cars on public roads. Drivers 1–4 all had a small amount of experience driving in a simulator. Driver 5 was a professional test driver with a great deal of experience driving simulated and real cars. The number and demographic range of test subjects is not sufficient to quantify the steering control behaviour of the population of drivers. However this was not the objective of the experiments. The driver model is intended to predict the behaviour of individual drivers. Increasing the number and demographic range of test subjects would increase confidence that the model could fit any driver from the population, but it is considered that the five subjects tested so far give sufficient confidence for further development of the model.

Practice runs of several of the trials were carried out before the experiment to familiarise the drivers with the steering task and the different disturbances and vehicle models. During the experiment the order of the trials was randomised. Before the experiment began each subject was told how the conditions may vary between the trials, however to avoid biasing their expectations they were not told anything about the specific conditions of each trial.

#### 4. Identification procedure

An identification procedure can be used to find values for the parameters of the new driver model presented in Section 2 which give the best possible fit to the results of the experiment described in Section 3. The identification procedure consists of two

**Table 2.** Experimental conditions for each trial (data also appears in [23])

Trial	Forcing function amplitudes			Vehicle	Preview
	$W_t$ (m*)	$W_v$ (m/s*)	$W_\omega$ (rad/s*)		
A1	1.58	0	0	F	<b>X</b>
A2	1.58	0	0	F	<b>✓</b>
A3	0	1.58	0	F	<b>0</b>
A4	0	0	1.58	F	<b>0</b>
A5	0	1.11	1.11	F	<b>0</b>
A6	0.79	0.79	0.79	F	<b>X</b>
A7	0.79	0.79	0.79	F	<b>✓</b>
A8	1.58	0	0	S	<b>X</b>
A9	1.58	0	0	S	<b>✓</b>
A10	0	1.58	0	S	<b>0</b>
A11	0	0	1.58	S	<b>0</b>
A12	0	1.11	1.11	S	<b>0</b>
A13	1.11	1.11	1.11	S	<b>X</b>
A14	1.11	1.11	1.11	S	<b>✓</b>

stages: Box–Jenkins identification to fit general polynomial transfer functions to the experimental results; and parametric identification to find a set of parameter values for the new driver model. The procedure is run separately for each of the five drivers. In addition, the measured steering angles are averaged over the five drivers to give a set of ‘averaged data’, which is also used for identification. The averaged data should contain less random noise compared with the data for the individual drivers, allowing an average set of parameter values to be found more reliably. However, it relies on the assumption that the drivers were using similar control strategies. The first 15 s of each trial are excluded from the data used for identification, as the drivers may have taken some time to work out the conditions of the trial and settle on a control strategy. The final 30 s of each trial are also excluded, so that the fit of the last 30 s can be measured to validate the predictive power of the model and to check for over-fitting (see Section 5.2).

#### 4.1. Box–Jenkins identification

The first identification stage involves fitting general transfer functions to the measured data to estimate the contribution of linear control behaviour to the measured steering actions. This gives an approximate upper bound on how well the parametric driver model could be expected to fit. The Box–Jenkins method is used to estimate polynomial transfer functions between each of the model inputs ( $f_t$ ,  $f_v$ ,  $f_\omega$ ) and the model output ( $\delta$ ) [24]. The method also finds a model of the noise spectrum  $H_n(s)$ . Polynomial transfer functions of order 5 are used to give a good fit to the measurements without over-fitting [25]. The Box–Jenkins method can also make allowances for time delays between each input channel and the output, however the method does not estimate these directly from the data so they have to be known in advance. To find optimal values of these time delays, Box–Jenkins identification is carried out with a range of different delays and a genetic algorithm is used to iterate towards values

**Table 3.** Parameters held constant for each step of the parametric identification procedure. (*sn*) refers to the value identified in step *n*.

Step	Trials	Values of parameters held constant										
		$q_\delta$	$V_a$	$V_\omega$	$V_p$	$W$	$\tau_{vi}$	$\tau_{ve}$	$T_t$	$T_p$	$\omega_{nm}$	$\zeta_{nm}$
1	A1, A3–A6, A8, A10–A13								0 s	0.1 s		
2	A1, A3–A6, A8, A10–13					(s1)×(noise ratio)			0 s	0.1 s		
3	A2, A7, A9, A14	(s2)	(s2)	(s2)		(s1)×(noise ratio)	(s2)	(s2)			(s2)	(s2)
4	A1–A14					(s1)×(noise ratio)			(s3)	(s3)		

which give the best fit to the experimental results.

#### 4.2. Parametric identification

The parametric driver model depends on eleven variable parameters which are neither fixed in advance nor taken from the experimental conditions. Ljung [24] presented two methods for identification of systems operating in closed-loop: direct identification where the system is simulated in open-loop and indirect identification where the system is simulated in closed-loop. As the feedback transfer function (the vehicle) is known in this case the indirect method is the most appropriate, and should result in lower bias than the direct method. The simulated steering angle  $\delta_{sim}$  can be compared with the measured steering angle  $\delta_{exp}$  and the mean-square difference minimised to find the optimum set of parameter values. This difference is composed of modelling error, which can be reduced by improving the accuracy of the model, and random noise introduced by the driver, which cannot be reduced.

If the driver noise is not white, bias may be introduced into the identification of the driver model. This bias can be reduced by filtering the prediction error so that the noise term approximates white noise [24]. This requires filtering by the inverse of the noise model  $H_n(s)$  (found in the Box–Jenkins identification procedure) to give a weighted prediction error  $\varepsilon$ . This amplifies the high frequencies, however the bandwidth of a driver’s steering control is physically limited. Therefore a low-pass filter is included, with a cutoff frequency of 30 rad/s, so that high-frequency errors are not penalised excessively:

$$\varepsilon(s) = \frac{1}{H_n(s)} \left( \frac{30}{s + 30} \right)^2 (\delta_{sim}(s) - \delta_{exp}(s)) \quad (13)$$

Previous studies have carried out simulations of similar identification procedures for driver models and shown that filtering by the inverse of the noise model is effective in reducing bias in the identified parameter values [25].

Finding the optimum set of parameter values involves minimising the mean-square weighted prediction error  $\varepsilon$ . Due to the number of parameters involved a stochastic method is required to explore the entire search space and find the global minimum solution. A genetic algorithm is therefore used, starting with a population of 100 random solutions and using principles of natural selection to ‘mate’ and ‘mutate’ the best solutions, allowing the population to converge towards the global minimum over 100 iterations [26]. A second minimisation stage is then carried out to focus in on the minimum using a gradient search method, taking the genetic algorithm solution as the starting point. The Matlab function *fmincon* is used for this stage with the *SQP*

algorithm.

Initially, single sets of parameter values are identified for each driver to fit the results of all trials. Minimisation over a multidimensional search space can be difficult, therefore the identification procedure is carried out in several steps to reduce the number of parameters identified at any one time. The conditions for each step are given in Table 3. In step 1 parameter values are identified for the trials without preview, with  $T_t$  and  $T_p$  held constant at 0 and 0.1 s. Parameters  $W$ ,  $V_a$ ,  $V_\omega$  and  $V_p$  affect not only the linear component of the modelled control strategy, but also the predicted amplitude and distribution of the random noise introduced by the driver. It is desirable for the noise amplitude predicted by the model to match the noise amplitude found in the experiment. The modelling error is assumed to be small, so that the driver noise is given by the difference between the measured steering angle  $\delta_{\text{exp}}$  and the modelled steering angle  $\delta_{\text{sim}}$ . Simulations show that the predicted noise amplitude is affected much more by the process noise than the measurement noise. Therefore, after step 1 the average ratio of the measured to the modelled noise amplitudes is found and used to scale  $W$ . In step 2,  $W$  is then held constant while the remaining parameter values are identified to fit the results of the non-preview trials once more.

In step 3, optimal values of  $T_t$  and  $T_p$  are found from the trials with preview. The value of  $V_p$  is also allowed to vary, because the overall level of uncertainty in the visual measurements depends on the number of preview points. The target shift  $T_t$  was found to be unnecessary for trials with the fast vehicle, so  $T_t$  is set to zero for trials A2 and A7. The other eight parameters are held constant at the values found in step 2. In step 4 a further optimisation is carried out, holding  $T_t$ ,  $T_p$  and  $W$  constant at the values found previously and identifying the remaining eight parameter values to minimise the average weighted prediction error across all fourteen trials.

Once a single set of parameter values is found to fit all of the trials as well as possible, separate parameter sets are identified for each trial individually. To reduce the number of parameters needing to be optimised, the values of  $T_p$ ,  $T_t$  and  $W$  are held constant, using the values found for the single parameter set. When running the parametric identification procedure for the averaged data, the value of  $W$  is given by the average of the values identified for the separate drivers, to give a realistic predicted noise amplitude.

## 5. Results and analysis

In the following subsections, the results of the experiment and the identification procedure are analysed in various ways. In Section 5.1 the agreement between the parametric driver model and the results of the experiments is investigated. In Section 5.2 the results are checked for signs of over-fitting to validate the model. The identified parameter values are compared between drivers in Section 5.3, and the noise levels predicted using these parameters are compared with those found in the experiment in Section 5.4.

### 5.1. Agreement between model and measurements

It is possible to quantify the agreement between the measured and modelled steering angles by calculating the ‘variance accounted for’ (VAF). This value represents the percentage of the variance in the measured signals  $\delta_{\text{exp}}$  which is matched by the model

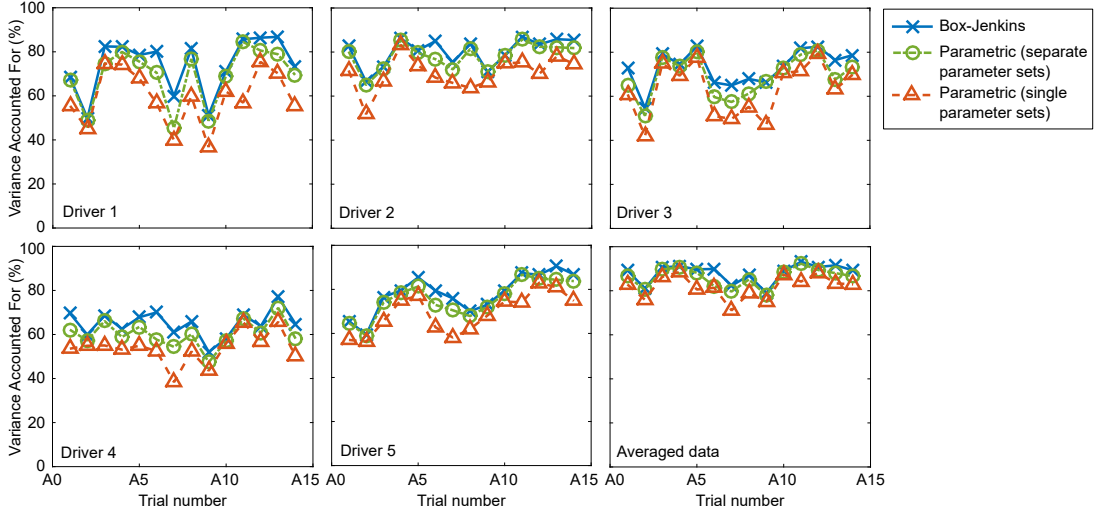


**Figure 7.** Agreement between driver model predictions and experimental data. VAF values are plotted for all five drivers and for the averaged data. The fit of the Box–Jenkins model is compared with the fit of the parametric driver model, either using separate parameter sets fit to each trial or a single parameter set to fit the results of all trials.

prediction  $\delta_{\text{sim}}$ , and is given by:

$$\text{VAF} = \left( 1 - \frac{\sum_k \{\delta_{\text{exp}}(k) - \delta_{\text{sim}}(k)\}^2}{\sum_k \{\delta_{\text{exp}}(k)\}^2} \right) \times 100\% \quad (14)$$

VAF values are plotted in Figure 7 to quantify the agreement between the predicted and measured steering angles for each of the five drivers as well as the averaged data.

As expected, VAFs are largest for the Box–Jenkins model, giving an approximate upper bound on the percentage of the steering signal which is linear. VAFs are lowest for the single parameter sets, as the separate parameter sets are able to get closer to the optimum for each individual trial. In general the VAFs for the separate parameter sets are very close to the VAFs for the Box–Jenkins model, indicating that the parametric model structure can explain the observed linear driver steering behaviour very well. VAFs for the single parameter sets are reasonably close to the VAFs for the separate parameter sets. For the individual drivers there are some trials where the single parameter sets do not fit as well, showing that the drivers’ individual control performance may change between trials, however the results using the single parameter set fit much better for the averaged data. The VAFs are higher for the averaged data than for the individual drivers, which is expected as averaging should reduce the amount of noise in the results. These VAF values are on average 98% of the Box–Jenkins upper bound using separate parameter sets, and 93% of the upper bound with a single set of parameters.

## 5.2. Model and procedure validation

Measurements from the last 30 s of each trial are not used in the identification procedure, but are kept to validate the predictive power of the different models and to check for over-fitting. If over-fitting had occurred, the model would fit the experimental results better for the data that was used for identification. To check this, average

**Table 4.** Average VAFs for signals between (a) 15–90 s and (b) 90–115 s

Driver	Box–Jenkins		Parametric (separate)		Parametric (single)	
	(a)	(b)	(a)	(b)	(a)	(b)
1	76.6	69.7	71.1	64.7	59.7	59.6
2	81.1	80.6	79.3	78.3	70.8	71.7
3	74.0	71.2	70.6	66.3	64.0	61.8
4	64.2	68.3	59.5	63.7	52.4	58.0
5	79.2	72.4	77.2	66.6	69.7	63.6
Averaged data	88.6	88.8	86.6	86.2	81.8	83.4

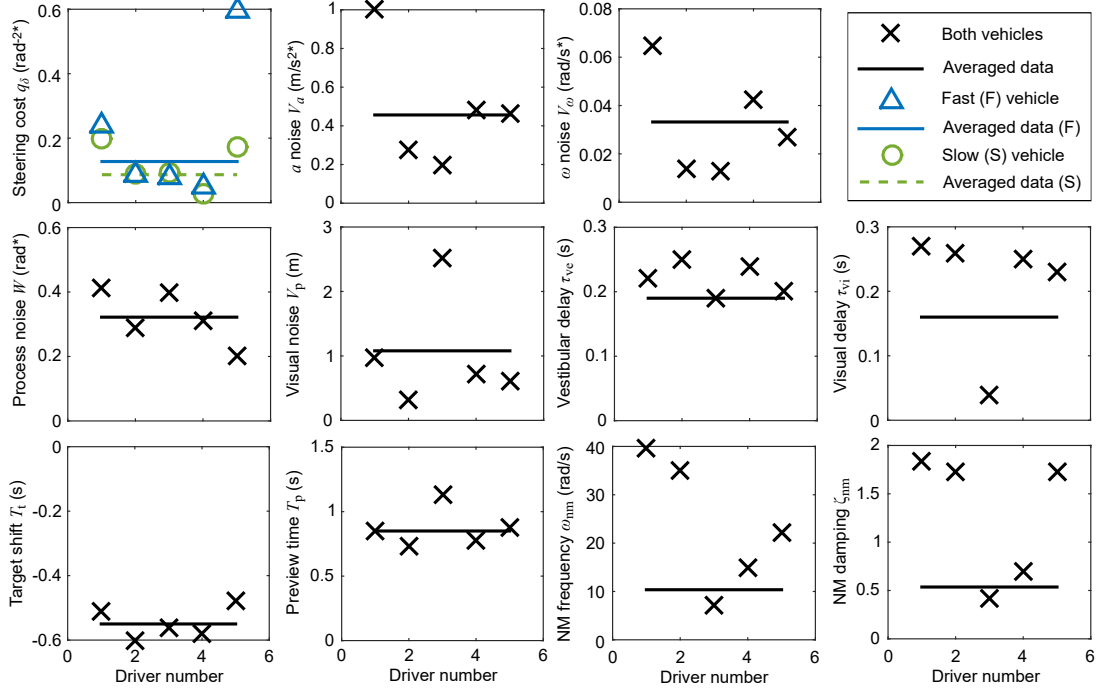
VAF values are calculated over all the trials for each driver, either for (a) the signals between 15 s–90 s (which are used for identification) or (b) the signals between 90 s–115 s. The results are compared for all three models in Table 4.

Table 4 shows evidence of some over-fitting in the Box–Jenkins results and the results for the separate parameter sets, as the average VAF is lower in the final 30 s for all drivers except driver 4 using these models. This is not seen for the averaged data, showing that the reduction in driver noise when averaging the measurements reduces the level of over-fitting. These results show that the VAFs given in Figure 7 for the Box–Jenkins model and single parameter sets may include a portion which is spuriously fitting to random variations in each trial. It also indicates that the separate parameter sets found for each trial may not always be reliable. In contrast, the results for the single parameter sets do not show any evidence of over-fitting. VAFs are lower in the last 30 s for drivers 3 and 5, but higher for drivers 2 and 4 and very similar for driver 1. This shows that by optimising over all of the trials any random variations are evened out, allowing a single set of parameter values to be found without fitting to noise in the results.

Simulated measurements were used to check that the identification procedure described reliably converges to the correct parameter values. Representative steering angles were created for each trial using the driver model with the parameter values identified for the averaged data over all trials. Measurement and process noise were added with the identified amplitudes, to give results with similar noise levels to the real measurements. An ensemble of ten sets of simulated results for each trial was created with different random noise signals, and the identification procedure was run for each set. The resulting identified parameter values demonstrated that in general the procedure does reliably converge to the correct parameter values. There was some slight variation, as to be expected when the measurements contain a significant amount of noise, however the identified parameters did not deviate substantially from their true values.

### 5.3. Identified parameter values

A comparison of the single parameter sets identified for each of the drivers is shown in Figure 8. In general the parameter values are similar between the different drivers, showing that the drivers were using similar control strategies. The parameter values found using the averaged data all fall within the range of the parameter values found



**Figure 8.** Single parameter sets found to fit all the trials. Values found for the individual drivers are shown by markers, and values found for the averaged data are shown by horizontal lines. Separate values of the steering cost  $q_\delta$  are identified for the fast and slow vehicles.

for the individual drivers, so the averaged data appears to be a valid representation of a typical driver’s steering control strategy.

The identified parameter values highlight various trade-offs between different parameters, which have similar effects on the modelled steering action. Comparison of the identified visual delay  $\tau_{vi}$  and neuromuscular frequency  $\omega_{nm}$  shows that drivers with lower values of one parameter also had lower values of the other. Decreasing the neuromuscular frequency increases the lag in the neuromuscular system, therefore this is compensated for by a reduction in the visual delay, although the vestibular delay is not affected. The neuromuscular damping  $\zeta_{nm}$  is also seen to decrease with  $\omega_{nm}$ .

One of the most significant differences between the drivers is in the steering cost  $q_\delta$ . This parameter describes the trade-off between steering effort and path-following error, and is a choice made by each of the drivers rather than a physical limitation. Some difference between the drivers is also seen in the process noise  $W$ , and this is discussed in Section 5.4. Due to the complexity of the model and the number of parameters, as well as the amount of noise in the measurements for each driver, the fact that the parameter values are a similar order of magnitude and in most cases close in value for the different drivers is encouraging. Further discussion is given in Section 6 to determine whether the identified values are physically appropriate.

#### 5.4. Measured and modelled driver noise amplitudes

One of the objectives of the identification procedure described in Section 4.2 is to find a set of parameter values which predicts driver noise levels similar to those seen in the experiments. This is achieved by scaling the process noise amplitude  $W$  based on the ratio between the measured and modelled noise amplitudes. The measurement noise

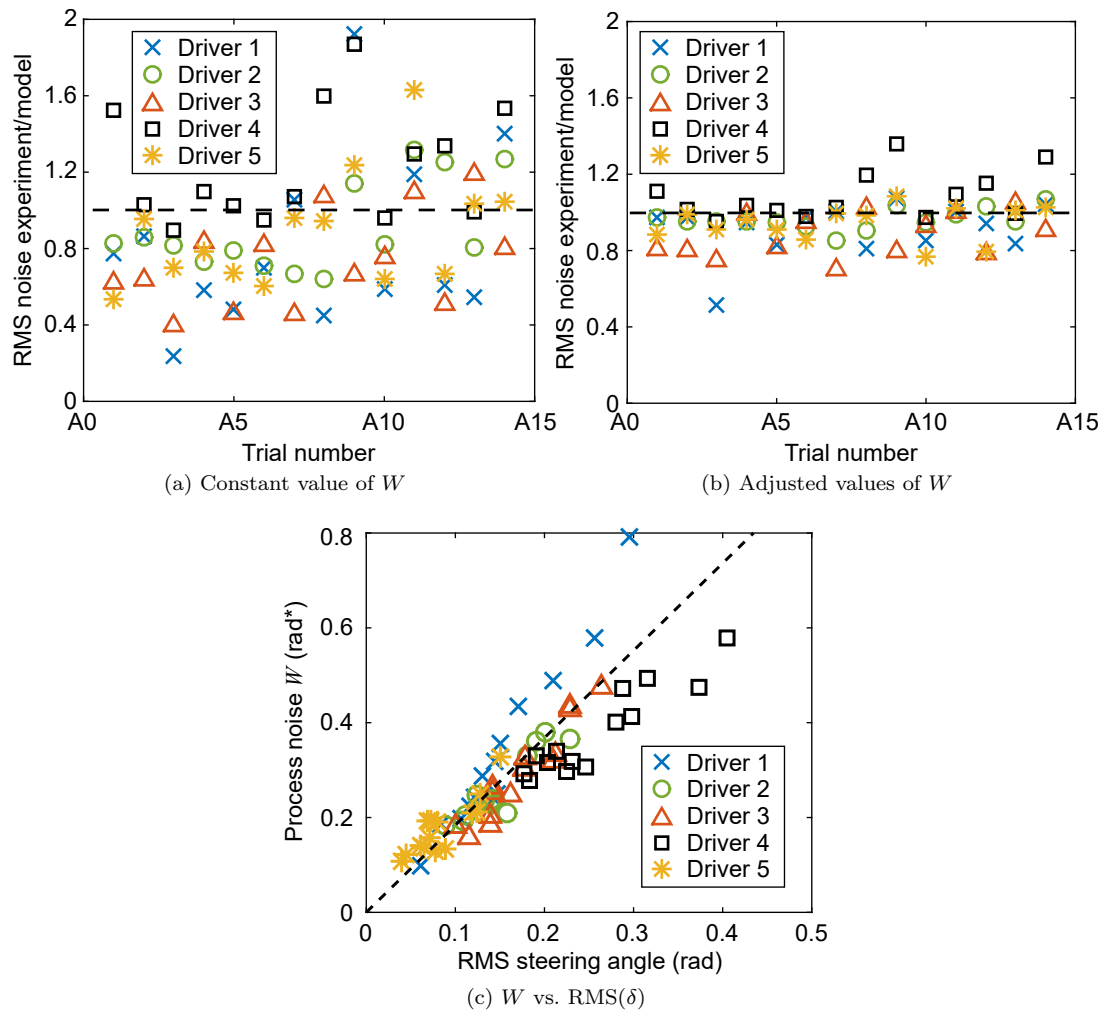


**Figure 9.** Ratio of measured and modelled RMS driver noise amplitudes. In (a), a constant value of  $W$  is used for each driver, whereas in (b) the values of  $W$  have been adjusted for each trial to match the noise levels more closely. In (c) adjusted values of  $W$  are plotted against RMS steering angle  $\delta$ .

amplitudes  $V_a$ ,  $V_\omega$  and  $V_p$  are not scaled; while the Kalman filter is able to reduce the effects of measurement noise by using other measurements and an internal model of the system, the process noise is added immediately before the plant so cannot be reduced as effectively by the driver. Simulations confirm that most of the noise in the modelled steering action originates from the process noise.

Assuming small modelling error, the driver noise is defined as  $(\delta_{\text{sim}} - \delta_{\text{exp}})$ . The ratio between the measured and modelled RMS noise amplitudes is shown in Figure 9a, using the single parameter sets identified for each driver. On average the noise amplitudes match well between the model and the experiment, with a ratio close to 1. There is a reasonable amount of variation between trials, with the experimental noise generally larger for the trials with the slow vehicle (A8–A14). To investigate the reasons behind the variation in noise amplitudes across the different trials, the values of  $W$  are scaled by the ratio of the experimental to the modelled RMS noise amplitudes (as shown in Figure 9a) for each trial, and the simulations are run again. The agreement between the measured and simulated steering angles is not affected, with the VAFs using the adjusted values of  $W$  on average 0.4% higher than the VAFs using a constant value of  $W$ . The resulting ratios between measured and modelled noise amplitudes are shown in Figure 9b. These ratios are much closer to 1 than those found using constant  $W$  values in Figure 9a.

The adjusted values of  $W$  are plotted against the RMS steering angle for each trial in Figure 9c. There is a clear linear relationship, showing that process noise is signal-dependent rather than additive. The amplitude  $\text{RMS}(\delta)$  of steering actions applied by the driver varies between trials and depends on the task and the driver’s internal cost function. Therefore it may be more appropriate to define a constant signal-to-noise ratio (SNR)  $\text{RMS}(\delta)/W$  between the RMS steering angle and the RMS process noise, rather than a constant value of  $W$ . Figure 9c shows that the SNRs are similar between the different drivers, with a value of 0.57 on average.

## 6. Discussion

The results presented in Section 5 can be used to give an insight into driver steering control behaviour and sensory systems during a realistic driving task, allowing knowledge of the underlying mechanics of human perception to be combined with understanding of the higher-level control strategies used while driving.

### 6.1. General discussion of results

Experimental data has been used to identify parameter values for a parametric driver model based on a physical understanding of human sensory dynamics. The VAF values presented in Section 5.1 show that the parametric model fits the experimental results almost as well as the upper bound given by the Box–Jenkins model. This result supports the hypothesis that driver steering control can be predicted using models of the underlying sensory mechanisms. The parametric model fits the results of all trials well with a single fixed set of parameter values. Simplifications have been made in the modelling of human sensory dynamics, such as neglecting visual perception of vehicle motion and assuming constant measurement noise on each previewed lateral displacement. The good agreement between the parametric model and experimental results shows that these assumptions are reasonable.

Another assumption made in the model is that the measurement and process noise is

**Table 5.** Comparison of identified parameter values with estimates from literature. Identified values are found using the averaged data.

Parameter	$q_\delta$ (fast)	$q_\delta$ (slow)	$V_a$	$V_\omega$	$V_p$	$W$	$\tau_{vi}$	$\tau_{ve}$	$T_t$	$T_p$	$\omega_{nm}$	$\zeta_{nm}$
<b>Units</b>	rad <sup>-2*</sup>	rad <sup>-2*</sup>	m/s <sup>2*</sup>	rad/s*	m	rad*	s	s	s	s	rad/s	–
<b>Identified</b>	0.13	0.087	0.46	0.033	1.1	0.32	0.16	0.19	-0.55	0.85	10	0.54
<b>Literature</b>	–	–	0.038	0.023	–	–	0.10–0.56	0.05–0.44	–	1	5.65–23.2	0.24–0.43

Gaussian, white and additive. In Section 5.4 the process noise  $W$  is found to correlate linearly with RMS steering angle, indicating that process noise is signal-dependent rather than additive. Signal-dependent noise could be included explicitly in the driver model [6], however this increases the complexity and computational requirements since the standard LQR and Kalman filter solutions are no longer optimal. As long as the conditions do not vary significantly over time a simpler solution is to choose additive noise amplitudes based on the expected average signal amplitudes.

Parameter values identified for each of the five drivers are found in Section 5.3 to be similar in general. No significant differences are found between a professional driver (driver 5) and normal drivers. This could be because the identified delays and noise amplitudes are linked to physical limitations which are similar in most healthy humans, so for simple tasks like those carried out in the experiment more experienced drivers do not necessarily have any advantage. The advantage of a professional driver is likely to be more apparent in the nonlinear handling regime near the limit of tyre adhesion, and in planning the optimum target trajectory.

## 6.2. Comparison of parameter values with literature results

A review of relevant literature relating to sensory dynamics during driving was carried out in [13], allowing the identified parameter values to be compared with results from the literature to determine whether the parametric driver model gives a realistic description of the function of sensory systems during driving. A comparison between the single set of parameter values identified to fit the averaged data and estimates from the literature is presented in Table 5.

There is some disagreement in the literature as to the values of delays in the visual and vestibular systems, and it can be difficult to distinguish between pure delays, lags and time taken to overcome threshold levels. Transmission of vestibular reflex signals has been found to be very fast [27], however other studies have suggested that neural processing of vestibular information may take longer than processing of visual information [28]. The identified vestibular delay of 0.19 s is slightly longer than the visual delay of 0.16 s, supporting the hypothesis that processing of vestibular information takes longer than visual information. Both of these values are within the (somewhat large) range suggested by results from the literature, and they can be used as a more specific estimate of sensory delays during driving.

Soyka et al. [29] developed a signal-in-noise model of sensory thresholds, which can be used to infer noise amplitudes from measured threshold data. Estimated noise amplitudes using this approach are compared with identified values in Table 5. The identified value of  $V_\omega$  is 1.4 times the value found from sensory threshold measurements, whereas the identified value of  $V_a$  is 12 times larger. Studies have found that vestibular thresholds may increase by factors between 1.5 and 6 during an active control task [7–10], which can explain the larger value of  $V_\omega$  but not of  $V_a$ . However, while the angular velocities in the experiment were very small and close to threshold levels,

the accelerations were much larger than the perception threshold. The ‘just noticeable difference’ for accelerations increases with stimulus amplitude [30], so the identified noise amplitude  $V_a$  may include signal-dependent as well as additive noise. Taking this into account, the identified noise amplitudes are plausible.

Studies measuring drivers’ gaze direction have found that drivers tend to look around 1 s ahead [3,31,32]. The identified preview time  $T_p$  is 0.85 s, which is slightly shorter than the 1 s found in the literature. This may be a result of the small target lateral displacements and the assumption of constant visual noise  $V_p$ , when in reality the target would become more difficult to see as the preview distance increases. The identified target shift  $T_t$  (which is only used for the slow vehicle) is 0.55 s, implying that the drivers steered 5.5 m ahead of the target on average. They may have aligned the front of the vehicle with the target rather than the centre of mass, although this cannot account for the full distance. Another explanation is that at low speeds the assumption of constant preview time could be invalid, and drivers look further ahead so that the preview distance isn’t too short.

The identified neuromuscular frequency  $\omega_{nm}$  is between values found for relaxed and tensed arms [22], however the identified damping ratio  $\zeta_{nm}$  is higher than the values found in both cases. In reality the driver’s neuromuscular system interacts in closed-loop with the spring-damper torque feedback of the steering wheel, however this interaction is not captured in the model. Therefore, the identified neuromuscular transfer function incorporates this complete closed-loop system, which acts as a low-pass filter between  $\hat{\delta}$  and  $\delta$ . While the transfer function for the neuromuscular dynamics in the model is intended to correspond to the dynamics of the driver’s arm muscles, it also plays a role in shaping the cost function. The steering cost is applied to  $\hat{\delta}$ , based on the hypothesis that the driver aims to minimise control inputs to the neuromuscular dynamics. However, the driver may have other costs, for example derivatives or filtered versions of  $\hat{\delta}$ , and these may come across in the identified neuromuscular parameter values.

Overall, comparison of the identified sensory parameter values with values found in the literature shows the identified values to be physically plausible. Although the identified noise amplitudes are larger than values inferred from sensory threshold measurements, this aligns with expectations during an active control task with multimodal sensory stimuli. The aim of the parametric driver model is to predict driver steering behaviour based on considerations of the physiological processes involved, so it is encouraging that the identified parameter values give a reasonable description of human sensory systems.

### ***6.3. Implications and limitations***

A model of driver steering control has been developed based on an optimal control strategy, incorporating models of the driver’s sensory dynamics. The model fits experimental results well, and identified sensory parameters are physically plausible when compared with measurements from the literature. These results support the hypothesis that drivers achieve close to the best possible control performance within the limitations of their sensory and motor systems. Experienced drivers will have spent many hours driving, allowing them to learn how best to use sensory information to control a vehicle. Increasing the number and demographic range of test subjects would increase confidence that the model could fit any driver from the population, but it is considered that the five subjects tested so far give sufficient confidence for further development

of the model.

The model gives a physical basis for the driver’s control decisions which is lacking in many existing models. Furthermore, this work has more general implications for the understanding of neuronal information processing during active control tasks. The identified time delays and noise parameters give an insight into the limitations of human sensorimotor systems in such a task, and how they compare with previous studies which have generally taken measurements under controlled, passive conditions. It is also shown that the processing carried out in the brain during an active control task such as driving can be modelled reliably by an optimal controller and state estimator.

The driver model presented in this paper has several limitations. The model is only derived for constant speed vehicles, and the yaw angle of the vehicle is assumed to be small. A linear vehicle model is used, which is a reasonable approximation for regular driving, however under more extreme conditions drivers may operate in the nonlinear region close to the limit of adhesion of the tyres. Driving simulator experiments with varying vehicle speed and nonlinear tyres may reveal greater differences in control behaviour between drivers than observed in the present experiments. The current optimal control approach to modelling the driver will likely require extension to represent the measured behaviour and differences between drivers. Nonlinear model predictive control is one possibility [12] but account may also need to be taken of non-optimal behaviour when the driver has not fully learnt the vehicle dynamics.

The current model is derived for random targets and disturbances, however further work is necessary to determine how drivers deal with more predictable or transient conditions. The derivation of the driver model assumes that there are no conflicts between the senses, and the experiment was carefully designed to allow the vehicle motion to be replicated at full scale. However, it is necessary to investigate how drivers behave when there are sensory conflicts, in particular when the motion is scaled or filtered. These limitations are addressed in further work [23].

## 7. Conclusion

A parametric model of driver steering control has been developed, incorporating human sensory dynamics and hypothesising that the driver’s control strategy is close to optimal within the limitations of their sensory and motor systems. Model predictions match experimental results from five test subjects well, with a ‘variance accounted for’ on average 98% of the upper bound on linear behaviour using separate parameter sets for each trial, and 93% of the upper bound with a single fixed parameter set. The identified parameter values are physically plausible compared with values from the literature. Identified vestibular delays are longer than visual delays, supporting previous studies which have suggested that processing of vestibular information takes longer than visual information. The identified process noise amplitude  $W$  is linearly correlated with the RMS steering angle  $\delta$ , showing that process noise is signal-dependent. The signal-to-noise ratio  $\text{RMS}(\delta)/W$  is consistent across the different trials and drivers, at around 0.57. Differences between the test subjects mainly resulted from different cost function weightings, and similar parameter values are identified for a professional driver to those found for less experienced drivers. Further work is necessary to address the limitations of the current model, considering nonlinear vehicles, more realistic road profiles and the effects of sensory conflicts on a driver’s control performance.

## Acknowledgement and data

This work was supported by the UK Engineering and Physical Sciences Research Council (EP/P505445/1, studentship for Nash). Supporting data are available at [doi.org/10.17863/CAM.1244](https://doi.org/10.17863/CAM.1244).

## References

- [1] MacAdam CC. Understanding and Modeling the Human Driver. *Vehicle System Dynamics*. 2003;40(1-3):101–134.
- [2] Plöchl M, Edelmann J. Driver models in automobile dynamics application. *Vehicle System Dynamics*. 2007;45(7-8):699–741.
- [3] Donges E. A Two-Level Model of Driver Steering Behavior. *Human Factors: The Journal of the Human Factors and Ergonomics Society*. 1978;20(6):691–707.
- [4] Sharp RS, Valtetsiotis V. Optimal preview car steering control. *Vehicle System Dynamics*. 2001;35(Suppl.1):101–117.
- [5] Cole DJ, Pick AJ, Odhams AMC. Predictive and linear quadratic methods for potential application to modelling driver steering control. *Vehicle System Dynamics*. 2006;44(3):259–284.
- [6] Bigler RS. Automobile Driver Sensory System Modeling Phd thesis. Cambridge University; 2013.
- [7] Pool DM, Valente Pais AR, De Vroome AM, et al. Identification of Nonlinear Motion Perception Dynamics Using Time-Domain Pilot Modeling. *Journal of Guidance, Control, and Dynamics*. 2012;35(3):749–763.
- [8] Valente Pais AR, Pool DM, De Vroome AM, et al. Pitch Motion Perception Thresholds During Passive and Active Tasks. *Journal of Guidance, Control, and Dynamics*. 2012;35(3):904–918.
- [9] Groen EL, Bles W. How to use body tilt for the simulation of linear self motion. *Journal of vestibular research : equilibrium & orientation*. 2004;14(5):375–385.
- [10] Rodchenko V, Boris S, White A. In-flight estimation of pilots’ acceleration sensitivity thresholds. In: *Modeling and Simulation Technologies Conference*; Reston, VA. American Institute of Aeronautics and Astronautics; 2000. p. e4292.
- [11] Groen E, Wentink M, Valente Pais A, et al. Motion Perception Thresholds in Flight Simulation. In: *AIAA Modeling and Simulation Technologies Conference and Exhibit*; Reston, VA. American Institute of Aeronautics and Astronautics; 2006. p. e6254.
- [12] Nash CJ, Cole DJ. Modelling the influence of sensory dynamics on linear and nonlinear driver steering control. *Vehicle System Dynamics*. 2018;56(5):689–718.
- [13] Nash CJ, Cole DJ, Bigler RS. A review of human sensory dynamics for application to models of driver steering and speed control. *Biological Cybernetics*. 2016;110(2-3):91–116.
- [14] Nash CJ, Cole DJ. Development of a novel model of driver-vehicle steering control incorporating sensory dynamics. In: Rosenberger M, Plöchl M, Six K, et al., editors. *The dynamics of vehicles on roads and tracks*. Graz, Austria: CRC Press; 2016. p. 57–66.
- [15] Zaal PMT, Pool DM, Mulder M, et al. Multimodal Pilot Control Behavior in Combined Target-Following Disturbance-Rejection Tasks. *Journal of Guidance, Control, and Dynamics*. 2009;32(5):1418–1428.
- [16] Timings JP, Cole DJ. Minimum Maneuver Time Calculation Using Convex Optimization. *Journal of Dynamic Systems, Measurement, and Control*. 2013;135(3):031015.
- [17] Butler JS, Smith ST, Campos JL, et al. Bayesian integration of visual and vestibular signals for heading. *Journal of Vision*. 2010;10(11):23.1–13.
- [18] Prsa M, Gale S, Blanke O. Self-motion leads to mandatory cue fusion across sensory modalities. *Journal of neurophysiology*. 2012;108(8):2282–2291.
- [19] Fetsch CR, Deangelis GC, Angelaki DE. Visual-vestibular cue integration for heading

- perception: applications of optimal cue integration theory. *The European journal of neuroscience*. 2010;31(10):1721–1729.
- [20] Wolpert DM, Ghahramani Z. Computational principles of movement neuroscience. *Nature neuroscience*. 2000;3:1212–7.
- [21] Telban RJ, Cardullo F. Motion cueing algorithm development: Human-centered linear and nonlinear approaches. NASA; 2005.
- [22] Pick AJ, Cole DJ. Dynamic properties of a driver’s arms holding a steering wheel. *Proceedings of the Institution of Mechanical Engineers, Part D: Journal of Automobile Engineering*. 2007;221(12):1475–1486.
- [23] Nash CJ, Cole DJ. Measurement and modelling of the effect of sensory conflicts on driver steering control. accepted for publication, *Journal of Dynamic Systems, Measurement and Control*. 2019;.
- [24] Ljung L. *System Identification: Theory for the User*. 2nd ed. Upper Saddle River, NJ: Prentice Hall; 1999.
- [25] Odhams AM, Cole DJ. Identification of the steering control behaviour of five test subjects following a randomly curving path in a driving simulator. *International Journal of Vehicle Autonomous Systems*. 2014;12(1):44–64.
- [26] Zaal PMT, Pool DM, Chu QP, et al. Modeling Human Multimodal Perception and Control Using Genetic Maximum Likelihood Estimation. *Journal of Guidance, Control, and Dynamics*. 2009;32(4):1089–1099.
- [27] Aw ST, Todd MJ, Halmagyi GM. Latency and initiation of the human vestibuloocular reflex to pulsed galvanic stimulation. *Journal of neurophysiology*. 2006;96(2):925–930.
- [28] Barnett-Cowan M. Vestibular perception is slow: a review. *Multisensory research*. 2013; 26(4):387–403.
- [29] Soyka F, Robuffo Giordano P, Beykirch KA, et al. Predicting direction detection thresholds for arbitrary translational acceleration profiles in the horizontal plane. *Experimental brain research*. 2011;209(1):95–107.
- [30] Naseri AR, Grant PR. Human discrimination of translational accelerations. *Experimental brain research*. 2012;218(3):455–464.
- [31] Land MF, Tatler BW. Steering with the head. *Current Biology*. 2001;11(15):1215–1220.
- [32] Chatterton M, Wilson M, Ashford D, et al. Eye–steering coordination in natural driving. *Experimental Brain Research*. 2007;180(1):1–14.